R. & M. No. 3529

MINISTRY OF TECHNOLOGY

AERONAUTICAL RESEARCH COUNCIL
REPORTS AND MEMORANDA

Boundary Layer Bleed Drag at Supersonic Speeds

By E. L. Goldsmith

LONDON: HER MAJESTY'S STATIONERY OFFICE
1968

PRICE 10*s.* 6*d.* NET

Boundary Layer Bleed Drag at Supersonic Speeds

By E. L. Goldsmith

Reports and Memoranda No. 3529*
April, 1966

Summary.

Four types of flow in boundary-layer bleeds are discussed. Expressions are given for calculating the bleed internal drag for the various types using two alternative definitions of drag. Some general curves are plotted which show the dependence of bleed drag on bleed pressure recovery and free stream Mach number. A number of calculated and measured bleed pressure recoveries are compared. Calculations have been made which show under what conditions there is no longer a performance advantage in 'burying' engines within the adjacent body or wing. Other calculations compare the drag obtained by ejecting the bleed air slowly (base bleed) with no boattailing on the nacelle and ejecting the air as a high speed flow combined with the concomitant boat-tailing.

LIST OF CONTENTS

*Replaces R.A.E. Tech. Report No. 66 143—A.R.C. 28320.

1. *Introduction.*

Intakes positioned on bodies or wings have the problem of dealing with the boundary layer on those surfaces. The boundary layer is subject to any pre-entry pressure rise of the intake and may thicken or separate, with undesirable effects on intake efficiency and stability of operation. It is usual, particularly at supersonic speeds (because of the magnitude of the overall pressure rise), to bleed or divert this boundary layer away from the intake before the start of the compression process. This means that a bleed or diverter drag has to be included in the total performance evaluation.

Since boundary-layer bleed air may be used in a variety of ways e.g. as cooling air for equipment or as a source of secondary air for an ejector propelling nozzle, it is often difficult to evaluate the precise drag penalty associated with this air. However by specifying bleed exit conditions, momentum calculations can be made to establish broad differences in drag as between various ways of dealing with the flow.

2. *Method of Calculation.*

2.1. *Types of Flow.*

Four types of flow through a bleed duct system can be distinguished: these are controlled by the exit area of the duct, internal shape near to the exit plane and conditions imposed at the exit by the internal flow. In the first place, the bleed duct may act in the same manner as a main engine air intake. A correct choice of exit area will enable the intake to run in its critical flow condition i.e. accepting the full flow defined by its entry plane area, with a normal shock positioned at the entry plane. Unless the pressure recovery of the duct is very low, the exit flow will be at sonic velocity at all supersonic free stream speeds except near $M = 1$.

A second type of flow is obtained by adding an expanding passage downstream of the choked minimum duct area. The bleed flow is then expanded down to free stream or possibly a base static pressure and discharged at supersonic velocity.

A third type of flow is that usually known as base bleed, in which the air is controlled to emerge at low subsonic velocity into a base region. In doing so it occupies a relatively large area and has a low total pressure. Various experiments[1,2] have shown that under these conditions the level of base pressure on any residual solid base area (and the static pressure at exit of the bleed air which is at the same value) can be appreciably higher than the level without base bleed. In one example base pressure ratio p_b/p_∞ for an axisymmetric body without boat-tail was raised from 0·6 to 0·8 at $M_\infty = 2{\cdot}0$.

Experiments at O.N.E.R.A.[3] and R.A.E.[4] at $M_\infty = 1{\cdot}90$ show that if an exit for base bleed is provided around the primary propulsive jet, the static pressure in the bleed air, $p_{BL_{ex}}$, can be not only higher than the level of base pressure without bleed, but actually above the level of p_∞, say around $1{\cdot}1\ p_\infty$. The level of exit pressure achieved depends on bleed mass flow and on the degree of expansion of the primary jet: in particular $p_{BL_{ex}}$ is highest when the primary jet is itself not fully expanded.

Calculations of bleed drag can be made for an arbitrary range of values of $p_{BL_{ex}}/p_\infty$ to show what values must be achieved to make this mode of ejection of the bleed air comparable with or better than the others discussed. The low bleed exit velocity means that bleed total pressure is low and for this reason the bleed internal drag may well be higher than for a process which involves minimizing total pressure loss. However, because the area occupied by the bleed air is much greater than that occupied in the higher total-pressure condition, a reduction in external drag may be obtained as a result of reducing or even completely eliminating a boat-tail.

The fourth system discussed is one in which the bleed flow is supersonic throughout the duct. If a constant-area duct is chosen then the only net force acting is internal skin friction: hence the internal drag can be calculated approximately in a fairly simple manner. The main problem with this case is the practical one of actually obtaining a supersonic through-flow. Supersonic internal flow will not be achieved if the build-up of boundary layer in the duct is such as to decelerate the flow so that it chokes at any station. Criteria for establishing the supersonic internal flow condition and experimental verification for constant area circular ducts in a uniform flow have been discussed in Ref. 5.

2.2. *Application of Momentum Equation.*

The basic expression for calculating internal drag is of course the same for all the above systems. It has been given before[6] for any air intake system in free-stream conditions.

The control surfaces chosen must be made consistent with definitions of engine thrust and external drag of the aircraft. A consistent system is illustrated in Fig. 1a. Engine thrust is given by:

$$-T = 2q_\infty A_\infty - \{(p_{ex} - p_\infty) + 2q_{ex}\} A_{ex} . \tag{1}$$

Bleed internal drag similarly is:

$$D_{BL_{int}} = 2q_\infty A_{BL_\infty} - \{(p_{ex} - p_\infty) + 2q_{ex}\} A_{BL_{ex}} . \tag{2}$$

Aircraft drag is the sum of wave drag and skin-friction drag of the portion shown shaded in Fig. 1a plus also the pre-entry drag associated with the exposed streamtube surfaces between station (∞) and the entry plane of the intakes.

Equation (2) however is not always the most convenient form. If a comparison was being made between a bleed duct and a boundary-layer diverter or if the drag of an auxiliary air intake was required, it would be more convenient to define aircraft drag as the wave and skin-friction drag of the shaded portion shown in Fig. 1b. In this case thrust would be given by:

$$-T = \{(p_l - p_\infty) + 2q_l\} A_{en} - \{(p_{ex} - p_\infty) + 2q_{ex}\} A_{ex} \tag{3}$$

(the suffix l indicates local 'free stream' conditions*) and bleed internal drag (from Ref. 7), by:

$$D_{BL_{int}} = \frac{\Phi'}{\Phi'_l} \{(p_l - p_\infty) + 2q_l\} A_{BL_{en}} - \{(p_{ex} - p_\infty) + 2q_{ex}\} A_{BL_{ex}} \tag{4}$$

where

$$\frac{\Phi'}{\Phi'_l} = \frac{\delta \int_0^{h/\delta} [(p - p_\infty) + \rho V^2] \, d\left(\frac{y}{\delta}\right)}{\delta \left(\frac{h}{\delta}\right) [(p_l - p_\infty) + \rho_l V_l^2]}$$

is the ratio of momentum flux in the boundary layer (to height h) to that in the local 'free stream' over the same height h.

2.3. *Evaluation of Equation* (2).

It is convenient to rewrite equation (2) as:

$$C_{D_{BL_{int}}} = \frac{D_{BL_{int}}}{q_\infty A_{en}} = \frac{2A_{BL_\infty}}{A_{en}} - \left\{ \left(\frac{p_{ex}}{p_\infty} - 1 \right) \frac{p_\infty}{q_\infty} + \frac{2q_{ex}}{P_{ex}} \cdot \frac{P_{ex}}{P_\infty} \cdot \frac{P_\infty}{q_\infty} \right\} \frac{A_{BL_{ex}}}{A_{en}} . \tag{5}$$

*The plane 'l' is taken to be at the intake entry plane and defines conditions of pressure and velocity on the body or wing at this station in the absence of the intake.

If now bleed exit flow conditions are specified, such as

(a) Sonic velocity at exit;

(b) expansion of the bleed flow in a divergent nozzle to $p_{ex} = p_\infty$; or

(c) ejection at low subsonic velocity at $p_{ex} = p_b$, it is possible to express the bleed drag in terms of bleed mass flow (as a proportion of main engine flow) and pressure recovery. Thus for case (a):

$$C_{D_{BL_{int}}} = 2\frac{A_{BL_\infty}}{A_{en}} - \left\{ \left(0{\cdot}5283 \frac{P_{BL_{ex}}}{P_\infty} \cdot \frac{P_\infty}{p_\infty} - 1 \right) \frac{p_\infty}{q_\infty} + 0{\cdot}7396 \frac{P_{BL_{ex}}}{P_\infty} \frac{P_\infty}{q_\infty} \right\} \frac{A^*_{BL_{ex}}}{A_{en}} \tag{6}$$

where $A^*_{BL_{ex}}$ is the sonic exit area for the bleed flow, so that:

$$\frac{A^*_{BL_{ex}}}{A_{en}} = \frac{A_{BL_\infty}/A_{en}}{\frac{P_{BL_{ex}}}{P_\infty} \cdot \frac{A_\infty}{A^*_\infty}}.$$

Similarly for case (b) when $p_{ex}/p_\infty = 1$.

$$C_{D_{BL_{int}}} = 2\left\{ \frac{A_{BL_\infty}}{A_{en}} - \left(\frac{q_{ex}}{P_{ex}} \right)_{BL} \frac{P_{BL_{ex}}}{P_\infty} \cdot \frac{P_\infty}{q_\infty} \frac{A_{BL_{ex}}}{A_{en}} \right\}. \tag{7}$$

The quantities $M_{BL_{ex}}$, $\left(\frac{q}{P}\right)_{BL_{ex}}$ and $\left(\frac{A^*}{A}\right)_{BL_{ex}}$ follow from an evaluation of:

$$\left(\frac{p}{P}\right)_{BL_{ex}} = \frac{p_\infty/P_\infty}{P_{BL_{ex}}/P_\infty}$$

and $\frac{A_{BL_{ex}}}{A_{en}}$ is of course $\left(\frac{A}{A^*}\right)_{BL_{ex}} \times \frac{A^*_{BL_{ex}}}{A_{en}}$.

For case (c) equation (5) applies where as before $M_{BL_{ex}}$ etc. follow from:

$$\left(\frac{p}{P}\right)_{BL_{ex}} = \frac{p_{BL_{ex}}/p_\infty}{\frac{P_{BL_{ex}}}{P_\infty} \times \frac{P_\infty}{p_\infty}}.$$

2.4. *Evaluation of Equation* (4).

It is shown in Ref. 7 that the ratio $\frac{\Phi'}{\Phi'_l}$ can be written as

$$\frac{\frac{\phi}{\phi_l}\gamma M_l^2 + \left(1 - \frac{p_\infty}{p_l}\right)}{\gamma M_l^2 + \left(1 - \frac{p_\infty}{p_l}\right)}$$

where

$$\frac{\phi}{\phi_l} = \frac{\delta \int_0^{h/\delta} \rho V^2 \, d\left(\frac{y}{\delta}\right)}{\delta \left(\frac{h}{\delta}\right) \rho_l V_l^2}$$

and is given in Fig. 5 of Ref. 7.

As for equation (2), equation (4) can be evaluated for the three exit flow conditions of sonic velocity, $p_{BL_{ex}} = p_\infty$ and $p_{BL_{ex}} = p_b$.

Assuming that the bleed runs 'full' i.e. that the bleed exit area is sufficiently large to pass all the flow in the boundary layer up to the full height of the bleed duct, equation (4) becomes:

$$C_{D_{BLint}} = \frac{D_{BL_{int}}}{p_\infty A_{en}} = \left[\frac{2\phi}{\phi_l}.\frac{q_l}{q_\infty} + \left(\frac{p_l}{p_\infty} - 1\right)\frac{p_\infty}{q_\infty}\right]\frac{A_{BL_{en}}}{A_{en}} - \left[\left(\frac{p_{ex}}{p_\infty} - 1\right)\frac{p_\infty}{q_\infty} + \frac{2q_{ex}}{q_\infty}\right]\frac{A_{BL_{ex}}}{A_{en}}. \tag{9}$$

Then for case (a), introducing sonic exit conditions as before:

$$C_{D_{BLint}} = \left[\frac{2\phi}{\phi_l}.\frac{q_l}{q_\infty} + \left(\frac{p_l}{p_\infty} - 1\right)\frac{p_\infty}{q_\infty}\right]\frac{A_{BL_{en}}}{A_{en}} - \left[\left(0{\cdot}5283\frac{P_{BL_{ex}}}{P_\infty}.\frac{P_\infty}{p_\infty} - 1\right)\frac{p_\infty}{q_\infty} + 0{\cdot}7396\frac{P_{BL_{ex}}}{P_\infty}.\frac{P_\infty}{q_\infty}\right]\frac{A^*_{BL_{ex}}}{A_{en}}. \tag{10}$$

The bleed duct mass flow is given by:

$$m_{bleed} = \left(\frac{m}{m_l}\right)m_l$$

where $m_l = \rho_l V_l A_{BL_{en}}$ and $\frac{m}{m_l}$ is the boundary-layer mass-flow ratio given in Fig. 1 of Ref. 7. This is a function of h/δ (bleed height in relation to boundary layer thickness) and the index of the power law distribution of velocity in the boundary layer.

Now

$$\frac{m}{m_l} = \frac{A_{BL_l}}{A_{BL_{en}}} = \frac{P_{BL_{ex}}}{P_l}.\left(\frac{A}{A^*}\right)_l.\frac{A^*_{BL_{ex}}}{A_{BL_{en}}}$$

(if it is assumed that $T_l = T_{BL_{ex}}$)
where A_{BL_l} is the area in the local 'free stream' that would be occupied at the local flow conditions of M_l and p_l by the boundary-layer flow into the bleed.

Thus equation (10) becomes:

$$C_{D_{BL_{int}}} = \left[2\frac{\phi}{\phi_l}\frac{q_l}{q_\infty} + \left(\frac{p_l}{p_\infty} - 1\right)\frac{p_\infty}{q_\infty}\right]\frac{A_{BL_{en}}}{A_{en}} - \left[\left(0{\cdot}5283.\frac{P_{BL_{ex}}}{P_\infty}.\frac{P_\infty}{p_\infty} - 1\right)\frac{p_\infty}{q_\infty} + 0{\cdot}7396\frac{P_{BL_{ex}}}{P_\infty}.\frac{P_\infty}{q_\infty}\right]\frac{\dfrac{m}{m_l}}{\dfrac{P_{BL_{ex}}}{P_l}.\left(\dfrac{A}{A^*}\right)_l} \tag{11}$$

3.2. *Bleed Flow.*

Rough estimates of boundary-layer thickness on slender wings can be made by treating the wing as a flat plate. The Reynolds number for any particular spanwise station is based on local distance from the wing leading edge and δ can be derived from the curves of C_f and θ/δ in Ref. 12. As shown in Fig. 6, except near to the centreline ridge, fair agreement between measurements[13] and simple estimates of this nature are obtained.

For the sake of simplicity in the calculations that follow it is assumed that the bleed is the full width of the nacelle entry and that the $h_{BL_{en}}/\delta = 1$. Thus as we have seen the bleed flow can be defined.

It should however be pointed out an aircraft designer may make a different choice of bleed geometry. Most experimental investigations of the variation of pressure recovery of a main intake with degree of immersion in the wing or fuselage boundary layer gives maximum pressure recovery at $h_{BL_{en}}/\delta$ values that are slightly below unity. Thus as bleed drag is proportional to bleed flow the optimum value of $h_{BL_{en}}/\delta$ is probably 0·7 to 0·8. The bleed also may not necessarily be the same width as the nacelle entry. A better drag compromise may be obtained by ducting the middle portion of the boundary-layer flow and diverting the outer portions.

4. *Calculations.*

4.1. *The Performance Advantage Obtained by Burying Engines.*

A comparison can be made of the drag of a buried engine installation with that of an isolated or podded nacelle i.e. it can be determined under what conditions (of bleed pressure recovery, bleed size and free stream Mach number) the boundary-layer bleed drag becomes comparable with the drag of an isolated nacelle.

The nacelle shown in Fig. 7 has been used for these calculations, positioned with its centreline 145ft (Case I) and 33ft (Case II) back from the wing leading edge.

It is assumed that in both cases the engine is buried in the wing to such an extent that, with the side walls of the nacelle parallel to the free stream, the top of the cowl adds no wave drag to the basic shape. The bleed is assumed to be the full width of the nacelle entry and $h_{BL_{en}}/\delta$ is taken to be 1·0.

The drag and proportions of an isolated axisymmetric nacelle with the same maximum cross sectional area, are shown in Fig. 8.

To be consistent as shown in Fig. 9 it is necessary to use equations (11) and (12) to calculate bleed drag, assuming $p_l = p_\infty$ and $M_l = M_\infty$. A comparison can then be made between the bleed drag for a nacelle having no incremental wave drag (Fig. 7) and the wave and skin-friction drag of a podded nacelle, which in turn has no bleed drag. It is assumed that the wave plus skin-friction drag of the strut connecting the podded nacelle to the wing can be roughly equated to the side wall skin-friction drag of the buried nacelle which is the only additional friction component in that case.

For Case I, with axial sonic discharge of the bleed air, Fig. 10 shows the influence of bleed-pressure recovery. The majority of the experimental results of Fig. 5 appear to give recoveries within 80 to 90 per cent of the theoretical normal shock value. A realistic figure for an actual installation will obviously depend on total wetted surface area in the duct, rates of diffusion, radii of curvature of bends etc. The effect of 10 deg isentropic compressive turning of the flow before the normal shock is also shown in this figure and should be compared with the result for 100 per cent theoretical normal shock recovery. A worthwhile gain is shown, corresponding to the improvement in bleed recovery given in Fig. 4.

Substantial reduction in bleed flow can be achieved by placing the engines further outboard from the aircraft centreline. A typical effect on drag is shown in Fig. 11 where Cases I and II are compared using 90 per cent of theoretical normal shock recovery (with sonic axial discharge). In the outboard position, of course, it may not be possible to submerge the necessary engine volume in the wing and hence the assumption of zero nacelle wave drag may be invalidated.

Further on Fig. 11 the effects of supersonic axial discharge are shown, as are also the results of a calculation of bleed drag assuming that the bleed flow is wholly supersonic. In this last case it has been assumed that the skin-friction drag is that appropriate to the free stream Mach number and Reynolds

number. The bleed runs the full length (40 ft) of the nacelle as shown in Fig. 7. As can be seen (for the case of high bleed flow) both these methods give increasing gains in performance over the result for sonic discharge as free-stream Mach number increases.

4.2. *Comparison of Subsonic (Base Bleed) and Supersonic Ejection of Bleed Air.*

Equation (8) can be evaluated for a particular bleed flow and a range of values for $p_{BL_{ex}}/p_\infty$ provided that the exit area for the bleed $A_{BL_{ex}}/A_{en}$ is known. A series of calculations for base bleed has been made, assuming that the maximum area of the nacelle and the area of the fully expanded nozzle are both known and that there is no boat-tailing, so that the area for base bleed is determined by the difference of these two.

$$A_{BL_{ex}}/A_{en} = A_{max}/A_{en} - A_j/A_{en}.$$

Hence if the primary jet exit area is reduced, corresponding to the jet being less than fully expanded, the base bleed exit area is correspondingly increased.

Results for a bleed flow of 5 per cent of the main intake flow at $M_\infty = 2{\cdot}2$ are shown in Fig. 12. If values of $p_{BL_{ex}}/p_\infty$ in the region 1·3 to 1·5 can be obtained, then negligible or even negative bleed drags can be obtained. However if this occurs only at low values of A_j/A_{max} there will be an appreciable loss of primary thrust due to the jet underexpansion.

In Fig. 13, some of the highest values for $p_{BL_{ex}}/p_\infty$ so far measured [3,4] are shown against a background of curves (similar to those of Fig. 12) calculated for $M_\infty = 1{\cdot}9$, the approximate Mach number of the test measurements If the change in gross thrust from the jet is now added to the bleed drag, Fig. 14 is obtained and indicates that in general there is no significant overall gain by underexpanding the main jet to increase bleed exit static pressure and hence reduce bleed drag.

Measured values of $p_{BL_{ex}}/p_\infty$ vary with bleed mass flow as shown in Fig. 15. However calculations of bleed drag indicate that in this particular configuration of constant-bleed exit area and varying bleed flow the minimum bleed drag is obtained at about $m_{BL}/m_j = 0{\cdot}02$ (Fig. 16).

Conditions at the bleed exit are shown in Fig. 17 and indicate that the flow is being ejected with low total head and at low velocity. These low values of total head are an automatic result of specifying bleed-flow exit area and exit static pressure. Physically they would be obtained by the bleed running super-critically so that supersonic flow developed in the bleed duct downstream of the entry until the resulting losses due to shockwaves and to boundary-layer effects were sufficient to reduce the total pressure ratio to the required level (0·1 to 0·17).

If the bleed duct is designed to minimize total pressure loss and the minimum choking area is chosen so that the bleed intake will run in a 'critical' flow condition, then from equation (7) the bleed drag can be calculated for the exit condition $p_{BL_{ex}} = p_\infty$. The area occupied by the bleed air can be arranged, as before, around the main jet, but in general, the bleed now occupies quite a small cross-sectional area, so that:

$$\frac{A_{max}}{A_{en}} = \frac{A_j}{A_{en}} + \frac{A_{BL_{ex}}}{A_{en}} + \frac{A_{base\ or\ boattail}}{A_{en}}.$$

Hence a further drag due to either a solid base or a boat-tail has now to be added.

Assuming a boat-tail to make up the difference between A_{max} and $(A_j + A_{BL_{ex}})$, it is possible to calculate its drag, for h given boat-tail angle, from two-dimensional flow considerations. In Fig. 18 the internal drag of the bleed is shown for various values of $P_{BL_{ex}}/P_\infty$. The area occupied by this air $A_{BL_{ex}}/A_{max}$ is also shown. For a given value of $P_{BL_{ex}}/P_\infty$ the drag due to a boat-tail which occupies the rest of the base area can now be added. Taking the value $P_{BL_{ex}}/P_\infty = 0{\cdot}3$ at $M_\infty = 2{\cdot}2$ and adding the drag due to boat-tailing, a comparison can be made (Fig. 19), between this configuration and the previously considered arrangement where all the residual base area was occupied with bleed air and there was no boat-tail. In the present example, it is seen that if the fully expanded nozzle occupies 0·7 of the maximum area of nacelle and the boat-tail angle is 5 deg, the arrangement with base bleed and no boat-tail gives the lower drag provided the exit pressure of the bleed air is greater than $1{\cdot}17\,p_\infty$. The corresponding minimum exit pressure when comparing with 10 deg boat-tail angle is $0{\cdot}98\,p_\infty$.

5. *Conclusions.*

1. Formulae are developed for the calculation of internal drag of a boundary-layer bleed, according to either of two definitions, to which correspond respectively two different definitions of external drag. Some general curves showing the variation of bleed drag with bleed pressure recovery have been given.

2. Measured and calculated bleed pressure recoveries show the same order of difference as exist between these two quantities for main engine air intakes.

3. Calculations show that if a nacelle is installed at the rear on the centreline of a typical large slender wing aircraft then the bleed drag can become equal to an isolated nacelle drag in the region $M_\infty = 2{\cdot}6$ to $2{\cdot}8$.

4. It would seem desirable to improve upon normal-shock recoveries for bleeds, particularly at Mach numbers in excess of $2{\cdot}0$. It has been shown that even 10 deg of isentropic compression leads to a substantial decrease in bleed drag.

5. If bleeds with isentropic internal supersonic flow can be developed then they appear to have a drag variation which drops with free stream Mach number and therefore may prove an attractive alternative to the diffuser type of bleed at higher Mach numbers.

LIST OF SYMBOLS

A	Cross-sectional area
A_{max}	Max cross-sectional area of nacelle $= 36{\cdot}25$ ft^2
$C_{D_{BL_{int}}}$	Bleed internal-drag coefficient $= \dfrac{D_{BL_{int}}}{q_\infty A_{en}}$
$C_{D_{ext}}$	External-drag coefficient (based on A_{max})
d, D	Duct diameters
d_e	Effective duct diameter $= \sqrt{\dfrac{4 A_{BL_{en}}}{\pi}}$
h	Bleed height
L, l	Duct lengths
M	Mach number
m	Mass flow
N	Index of power law velocity distribution
P	Total pressure
p	Static pressure
q	Dynamic pressure
s	Local semi-span
T	Stagnation temperature
V	Velocity
w	Bleed width

y	Spanwise co-ordinate
β	Duct diffusion angle
γ	Ratio of specific heats C_p/C_v
δ	Boundary-layer height
ρ	Density
ϕ, Φ	Boundary-layer momentum functions (from Ref. 7)
θ	Angle of ejection of bleed air
$()_\infty$	Free stream
$()_l$	Local conditions
$()_{BL}$	In the bleed duct
$()_{BL_{en}}$	Bleed entry
$()_{BL_{ex}}$	Bleed exit
$()_{en}$	Intake entry
$()_{ex}$	Nozzle exit
$()_b$	Base

LIST OF REFERENCES

1 J. Reid, R. C. Hastings .. The effect of a central jet on the base pressure of a cylindrical afterbody in a supersonic stream.
A.R.C. R. & M. 3224. December 1959.

2 E. M. Cortright, ... Preliminary investigation of effectiveness of base bleed in reducing
A. H. Schroeder .. .. drag of blunt-base bodies in supersonic stream.
NACA RM E51A26. March 1951.

3 J. Leynaert, J.-M.Brasseur .. Problemes d'aerodynamiques inteme poses par l'avione transport supersonique 'Mach 2' – (Vime Congress Aeronaut que European Venix 12–15 September 1962). *La Récherche Aéronautique* No. 91 Nov.–Dec. 1962, pp. 15 to 22, and private communication of additional data.

4 M. M. Shaw .. .. .. The effect of base bleed on the base pressure of several shrouded and unshrouded propelling nozzles at $M_\infty = 1{\cdot}96$.
R.A.E. Tech. Report 66 182. June 1966.

5 J. Seddon .. .. .. The flow through short straight pipes in a compressible viscous stream.
A.R.C., CP 355. April 1955.

6 L. E. Fraenkel .. .. .. The external drag of some pitot-type intakes at supersonic speeds Part I.
R.A.E. Report Aero 2380, A.R.C. 13537. June 1950.

7 P. C. Simon, K. L. Kowalski .. Charts of boundary-layer mass flow and momentum for inlet performance analysis, Mach number range 0·2 to 5·0.
NACA Tech. Note 3583. November 1955.

8 R. G. Huff, A. R. Anderson .. Internal performance of several auxiliary air inlets immersed in a turbulent boundary layer at Mach numbers of 1·3, 1·5 and 2·0.
NACA RM E56J18. January 1957.

9 P. C. Simon .. .. .. Internal performance of a series of circular auxiliary air-inlets immersed in a turbulent boundary layer, Mach number range 1·5 to 2·0.
NACA RM E54L03. March 1955.

10 D. P. Hearth, ... Investigation at supersonic and subsonic Mach numbers of
R. W. Cubbison .. .. auxiliary inlets supplying secondary air-flow to ejector exhaust nozzles.
NACA RM E55J12a. January 1956.

11 J. W. Cnossen .. .. .. Unpublished U.S. Report.

12 W. F. Cope .. .. .. Notes of graphs for boundary layer calculations in compressible flow.
A.R.C. CP 89. August 1951.

13 A. W. Sharp .. .. .. Some recently boundary layer measurements on a slender delta wing at supersonic speeds.
A.R.A. Aero Memorandum No. 25.

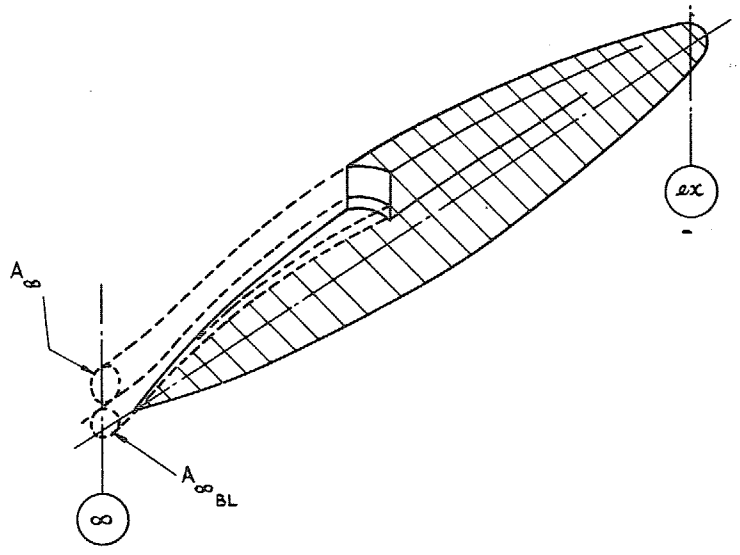

FIG. 1 (a)

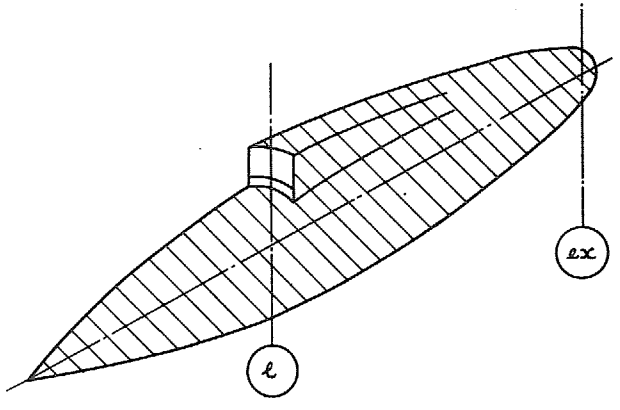

FIG. 1 (b)

FIG. 1. Definition of stations for momentum equation

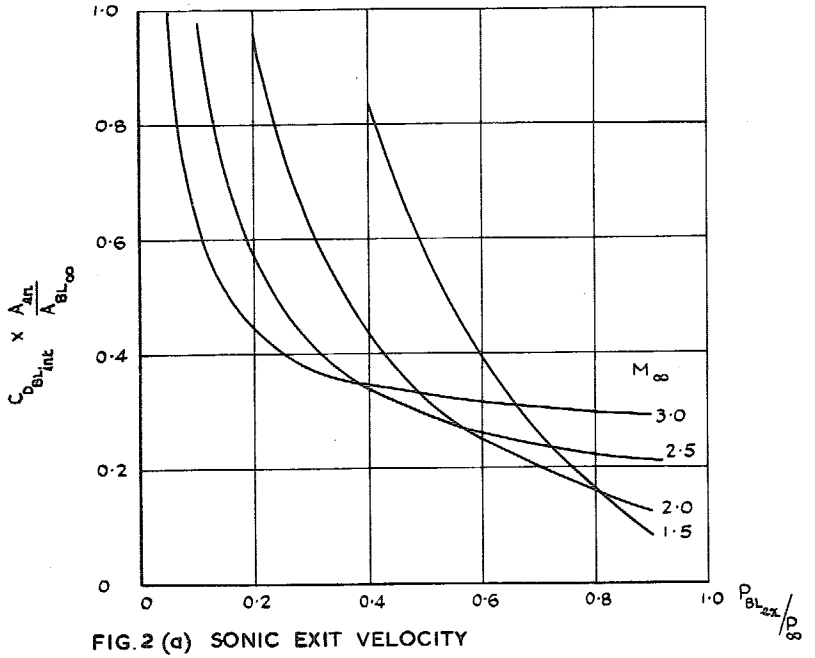

FIG. 2 (a) SONIC EXIT VELOCITY

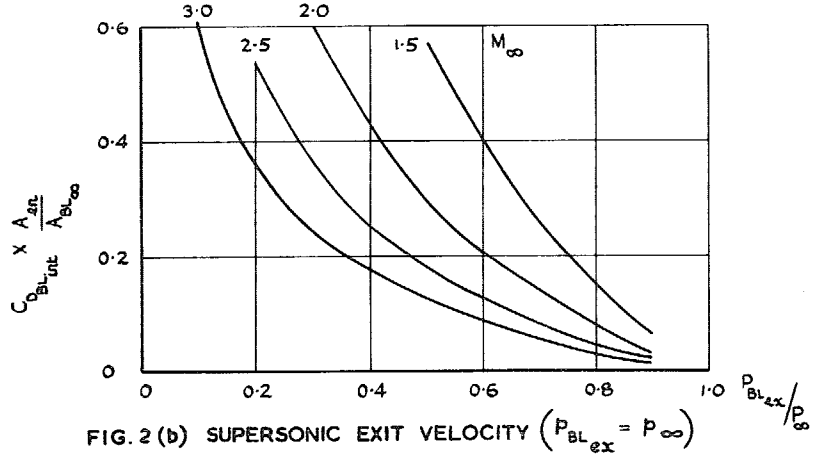

FIG. 2 (b) SUPERSONIC EXIT VELOCITY ($P_{BL_{ex}} = P_\infty$)

FIG. 2. Variation of $C_{D_{bleed}} \Big/ \frac{A_{BL_\infty}}{A_{en}}$ with Mach

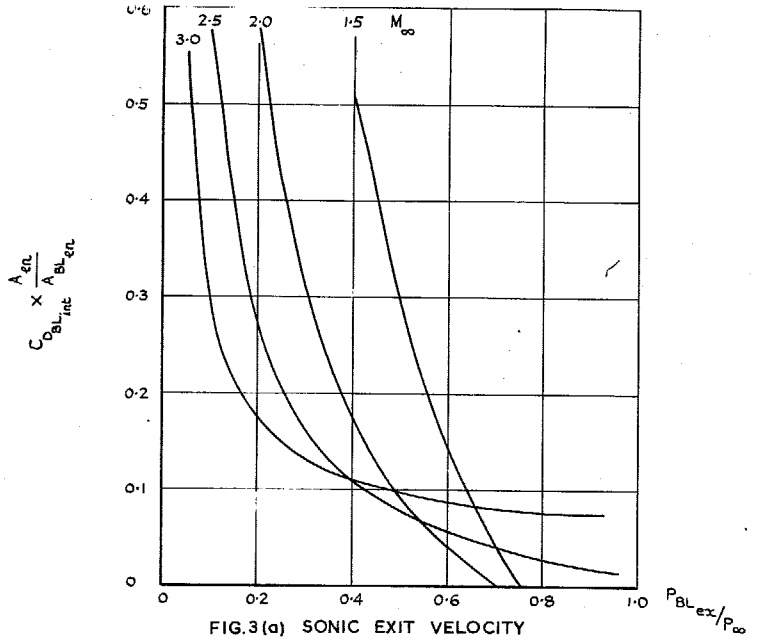

FIG. 3 (a) SONIC EXIT VELOCITY

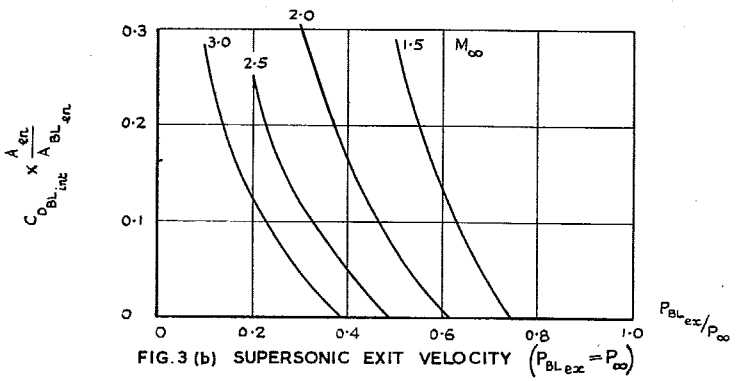

FIG. 3 (b) SUPERSONIC EXIT VELOCITY $\left(P_{BL_{ex}} = P_\infty\right)$

FIG. 3. Variation of $C_{D_{\text{bleed}}} / \frac{A_{BL_{en}}}{A_{en}}$ with Mach number and bleed total pressure.

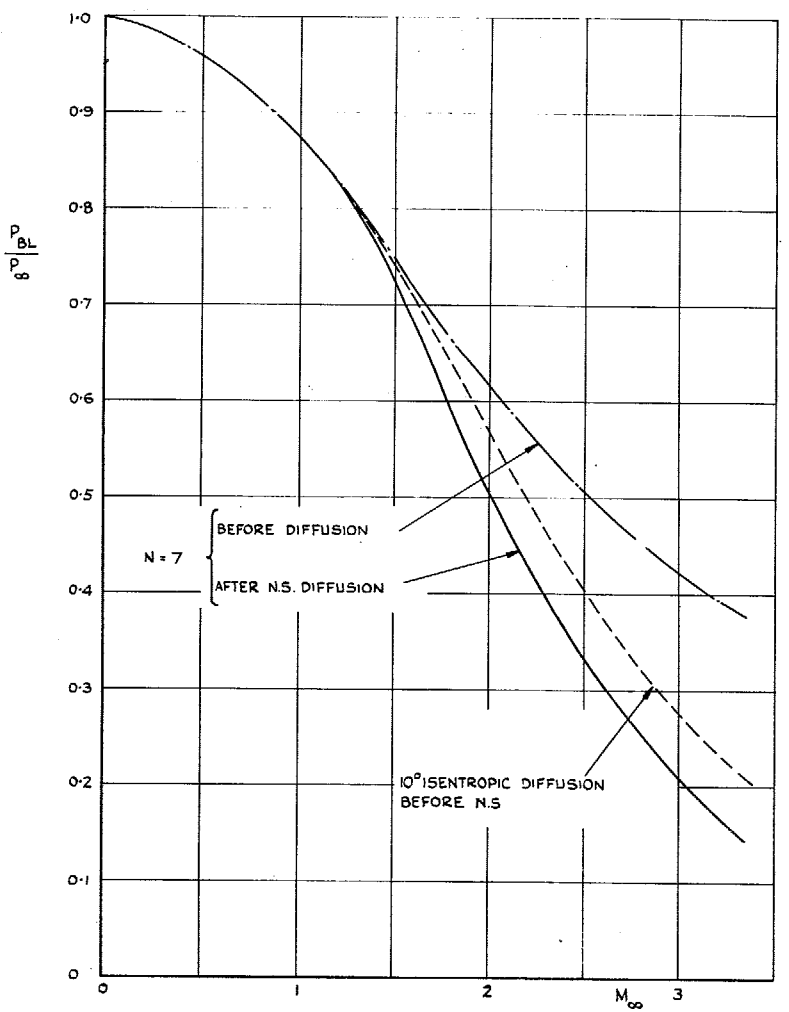

FIG. 4. Theoretical total pressure in a boundary layer ($N = 7$) before and after normal shock diffusion and the effect of some isentropic diffusion before the normal shock.

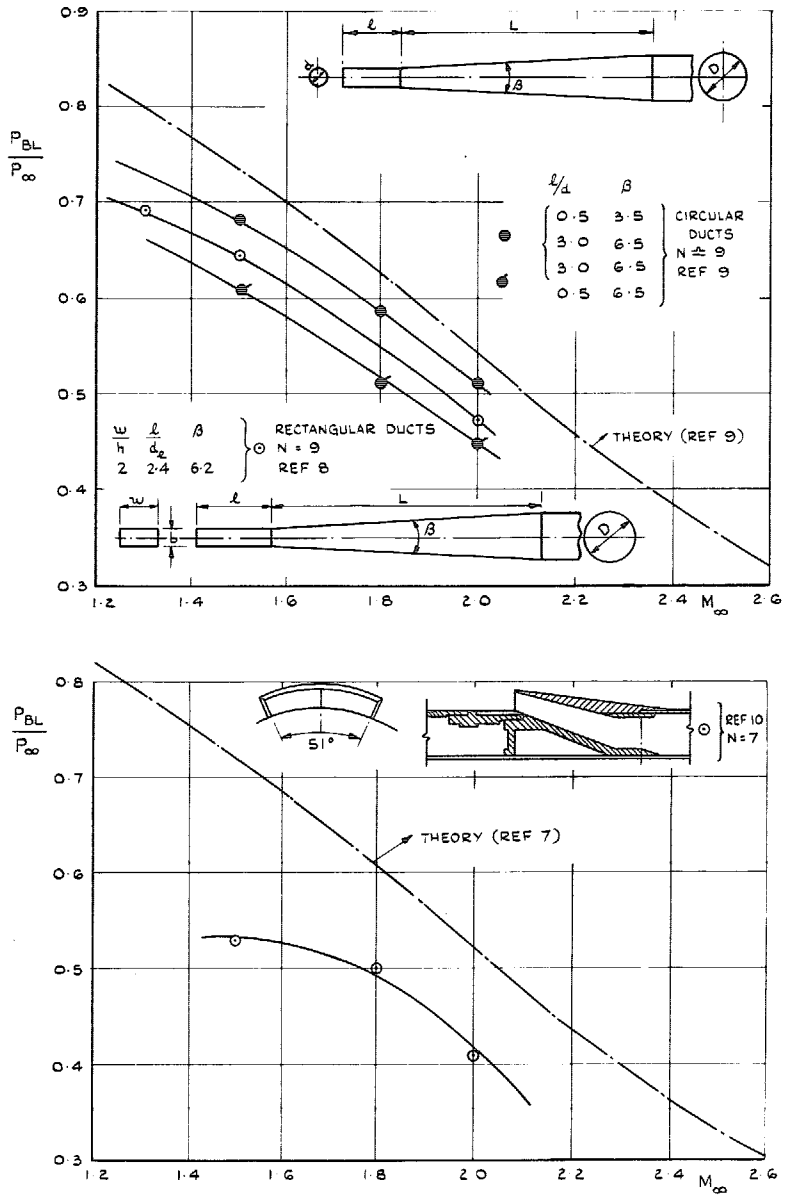

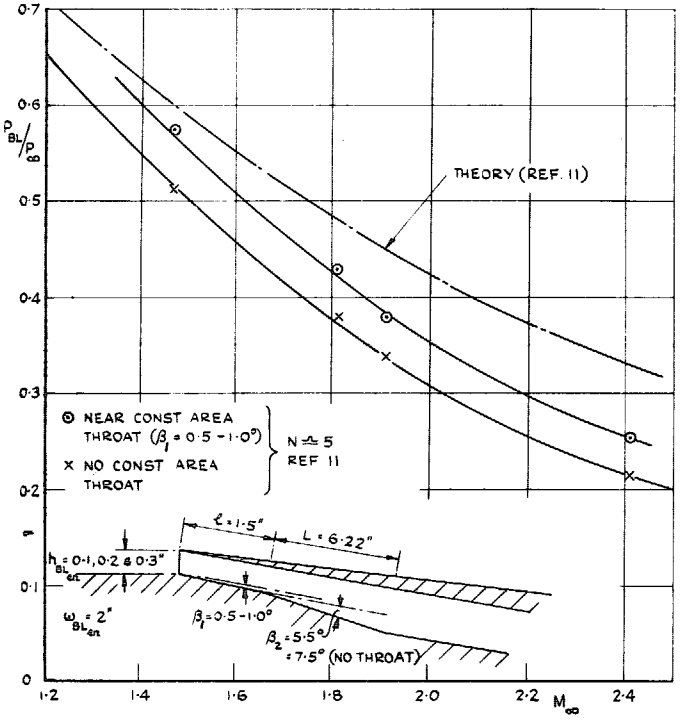

FIG. 5. Typical measured pressure recoveries

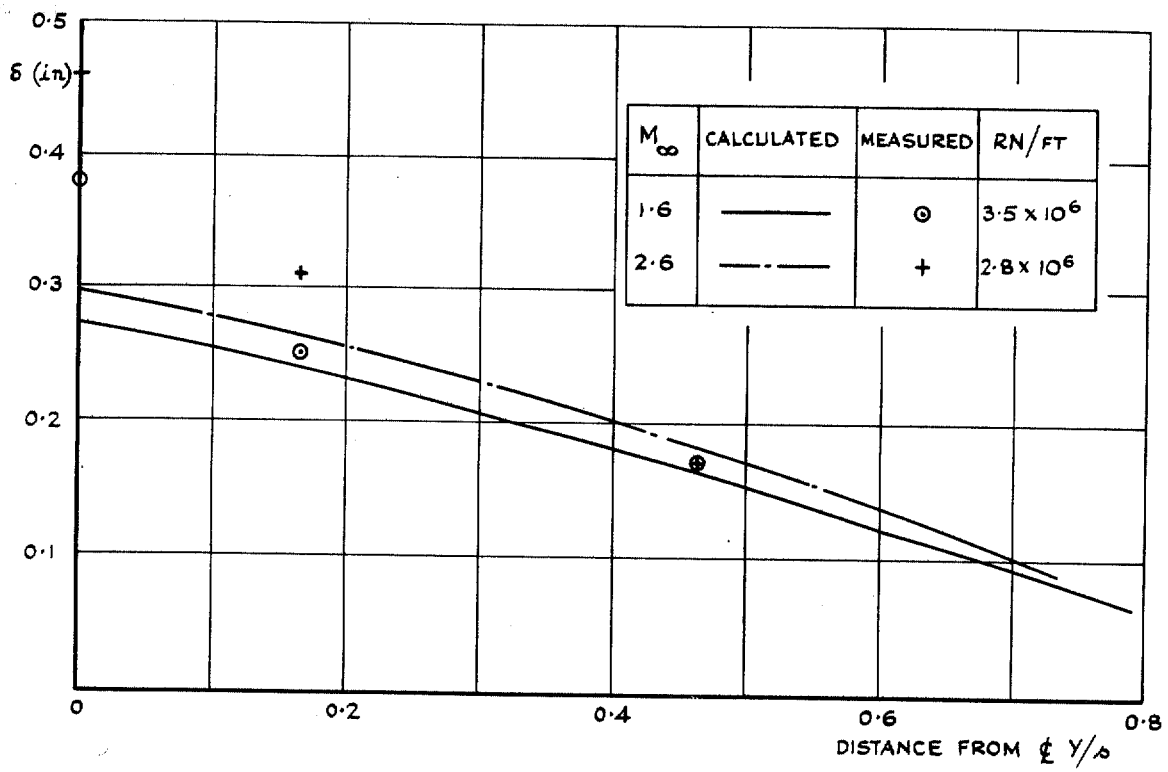

FIG. 6. Comparison of measured and calculated boundary-layer thickness for symmetrical delta wing.

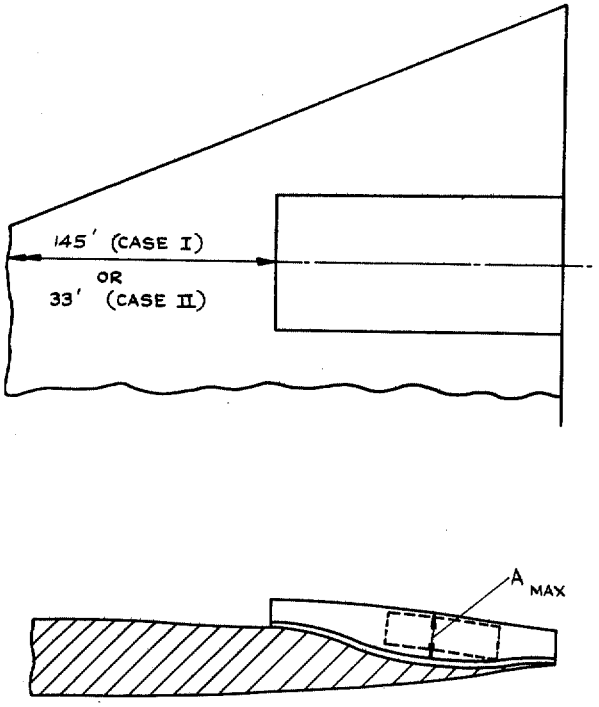

FIG. 7. 'Buried' engine nacelle geometry.

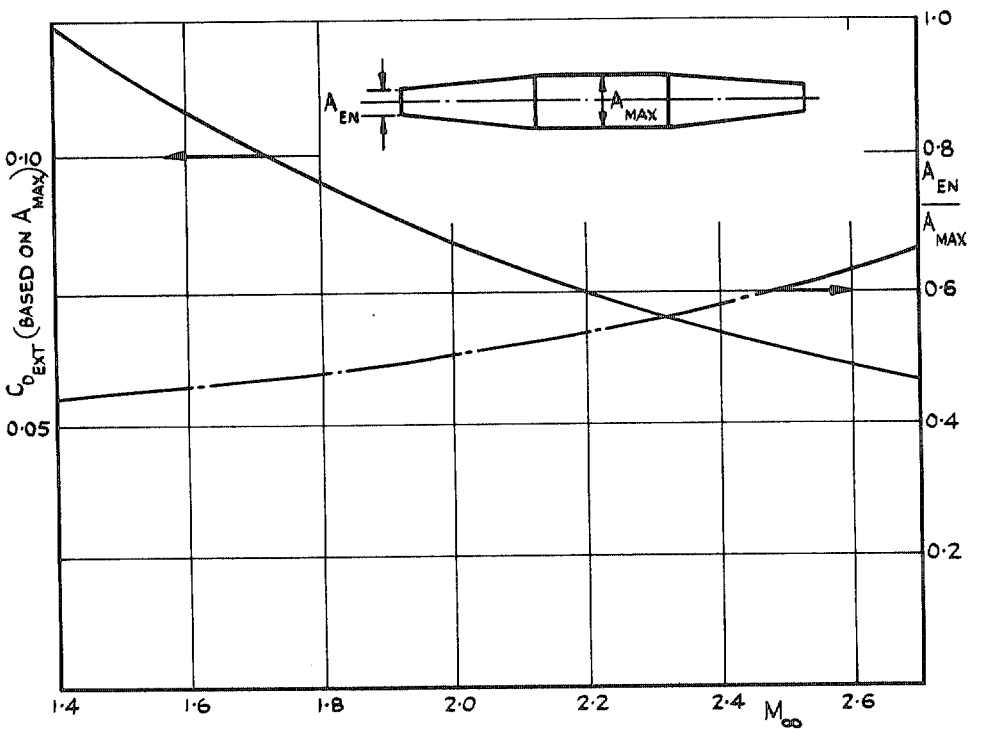

FIG. 8. Basic nacelle proportion and drag.

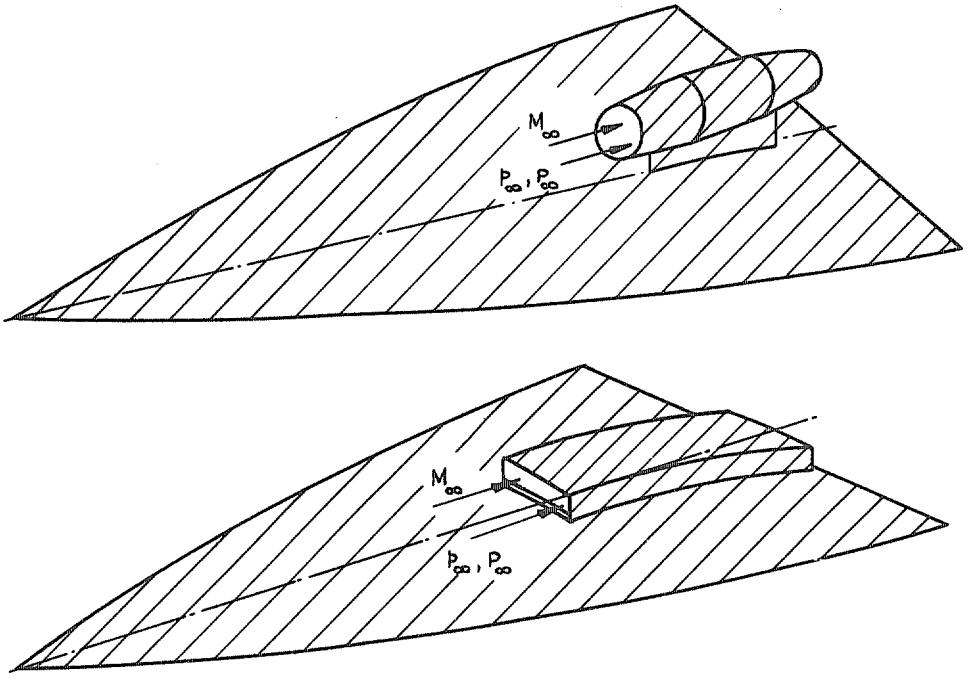

FIG. 9. Comparative configurations, 'buried' and 'podded' engine installations. (Aircraft external drag surface shown shaded).

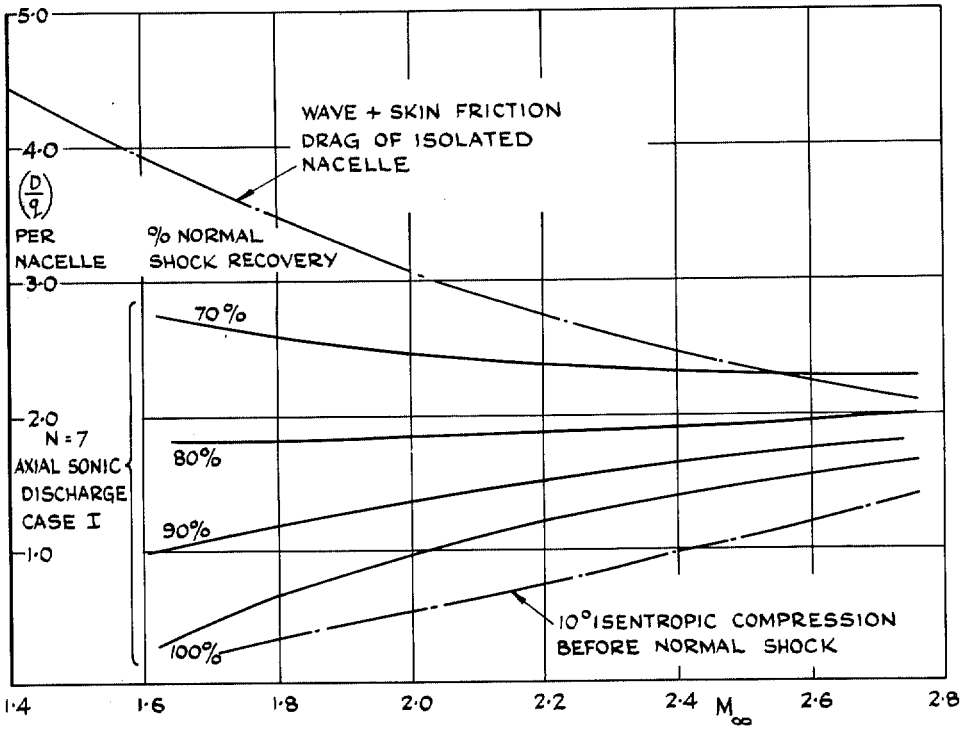

FIG. 10. Variation of bleed drag with bleed-pressure recovery.

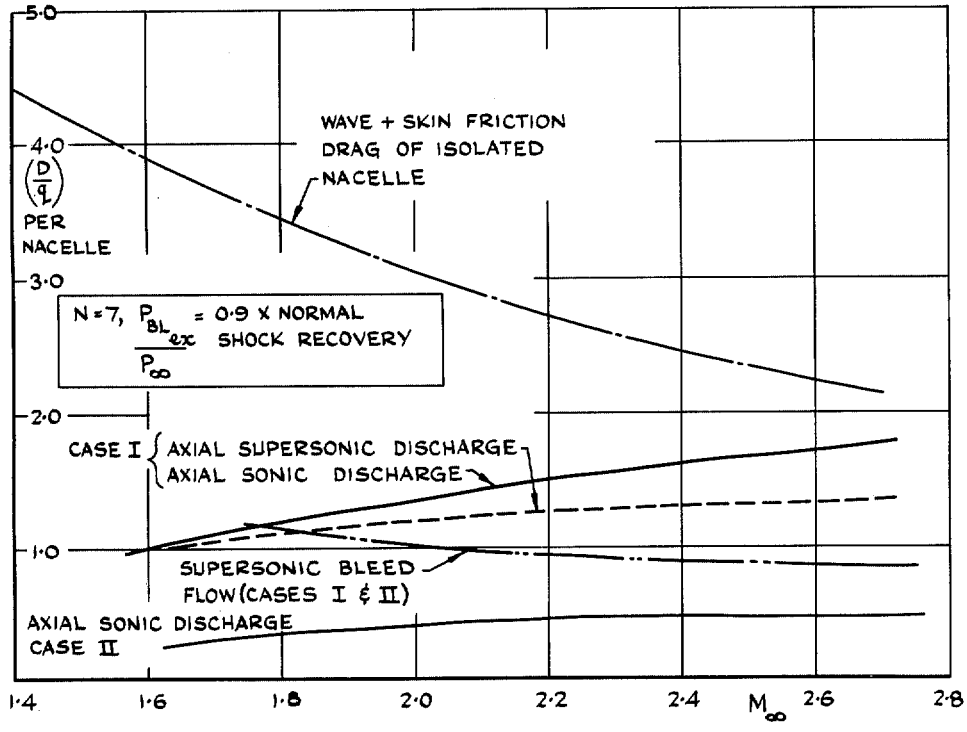

FIG. 11. Comparison of drag of buried and podded engine installations.

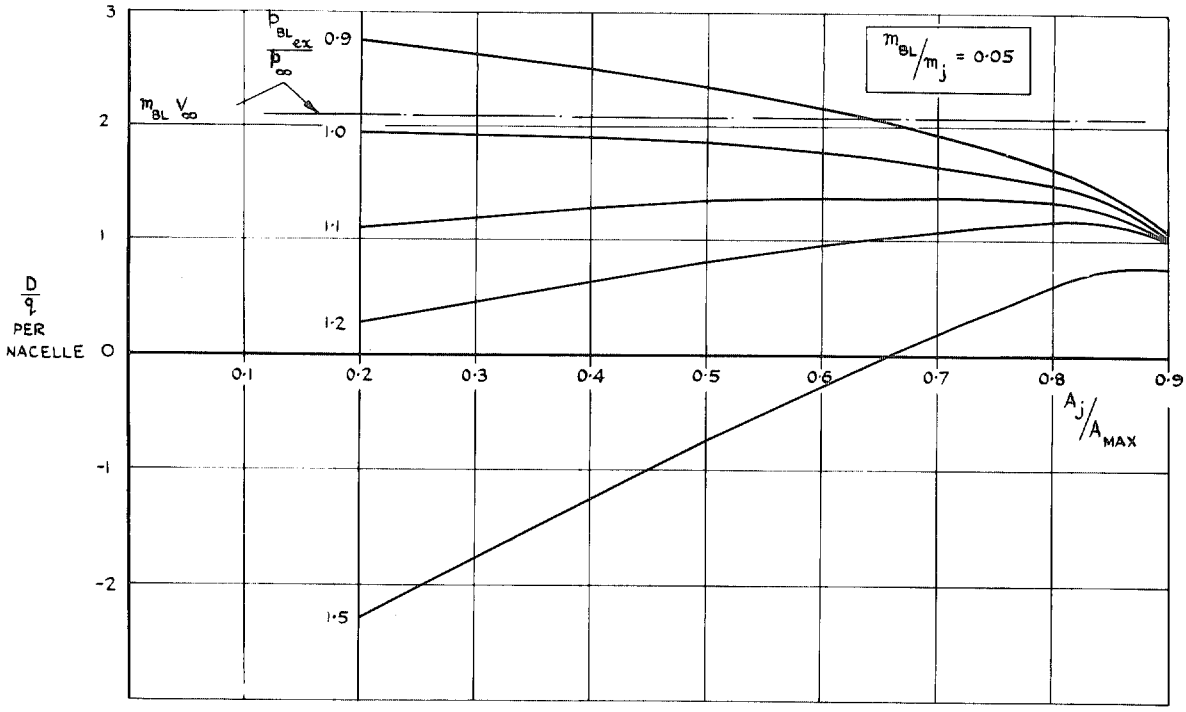

FIG. 12. Boundary-layer bleed drag at $M_\infty = 2{\cdot}2$.

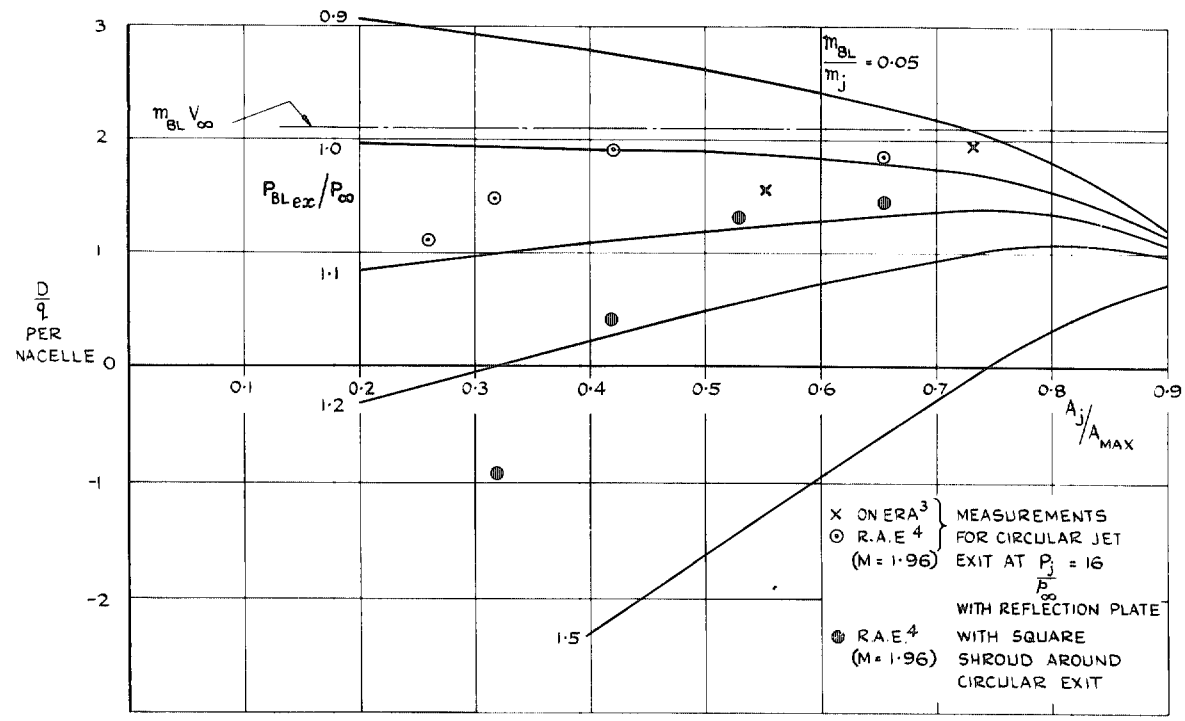

FIG. 13. Boundary-layer bleed drag at $M_\infty = 1{\cdot}9$.

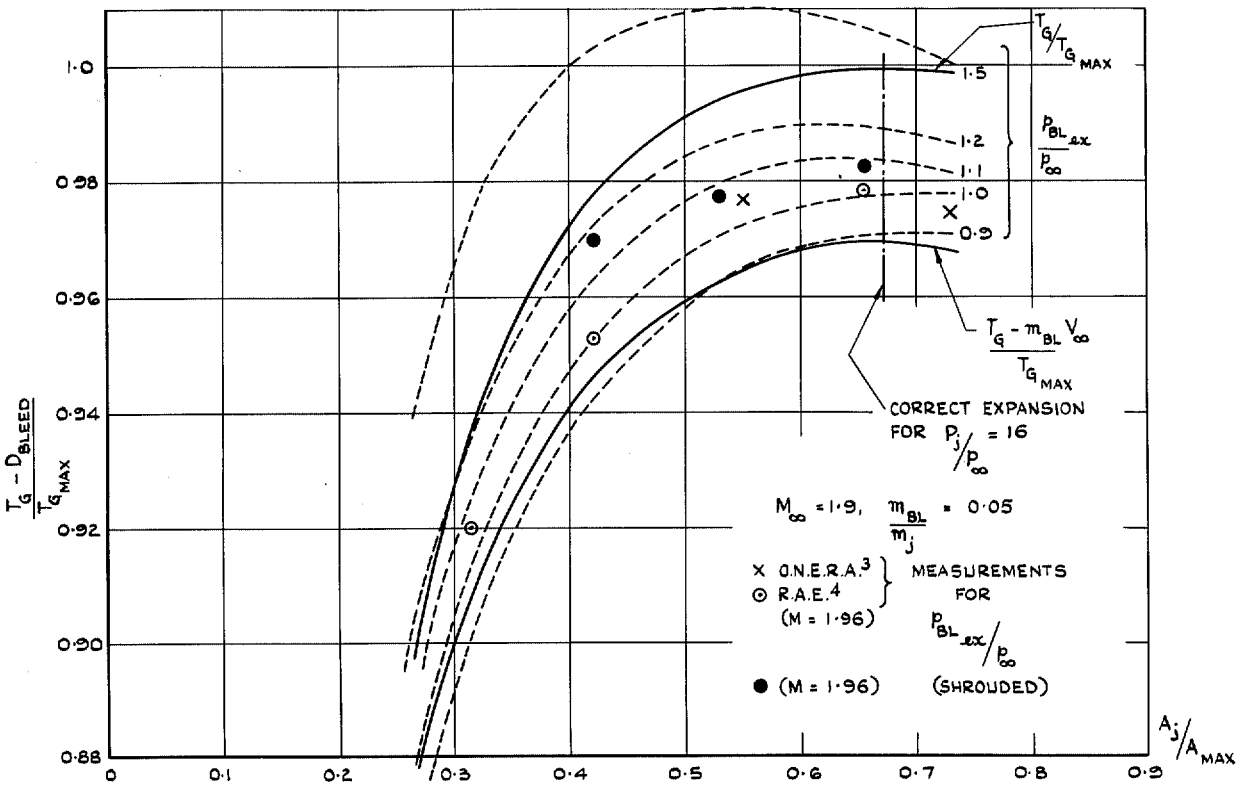

FIG. 14. Variation of gross thrust minus bleed drag with jet exit area at $M_\infty = 1·9$.

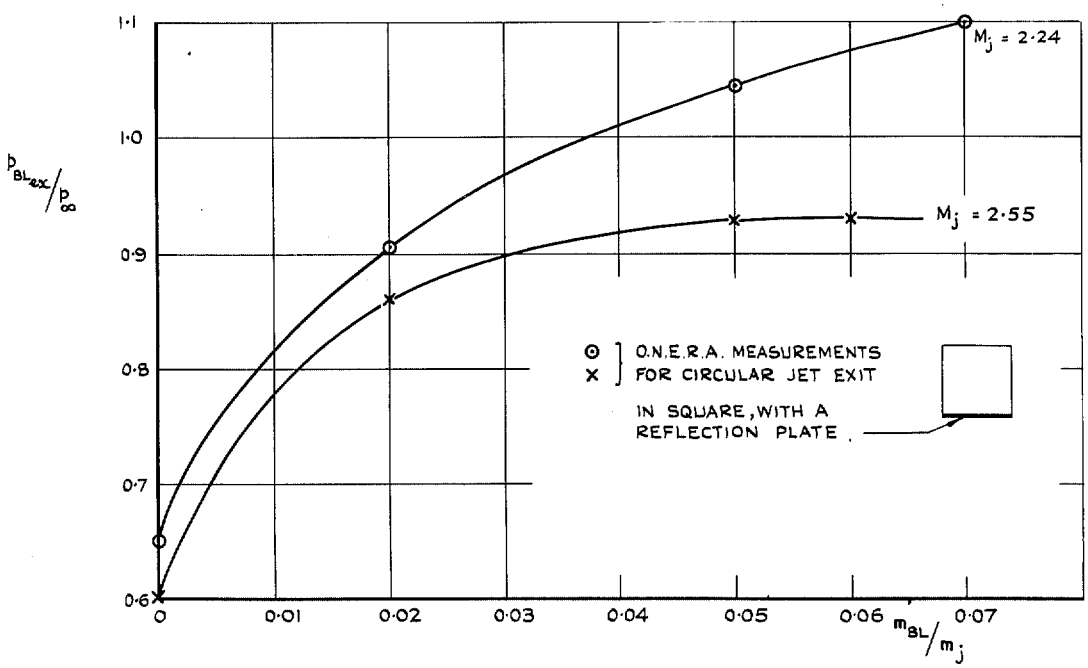

FIG. 15. Variation of $p_{BL_{ex}}/p_\infty$ with bleed mass flow and design Mach number of the main jet nozzle. $(P_j/p_\infty = 16)$.

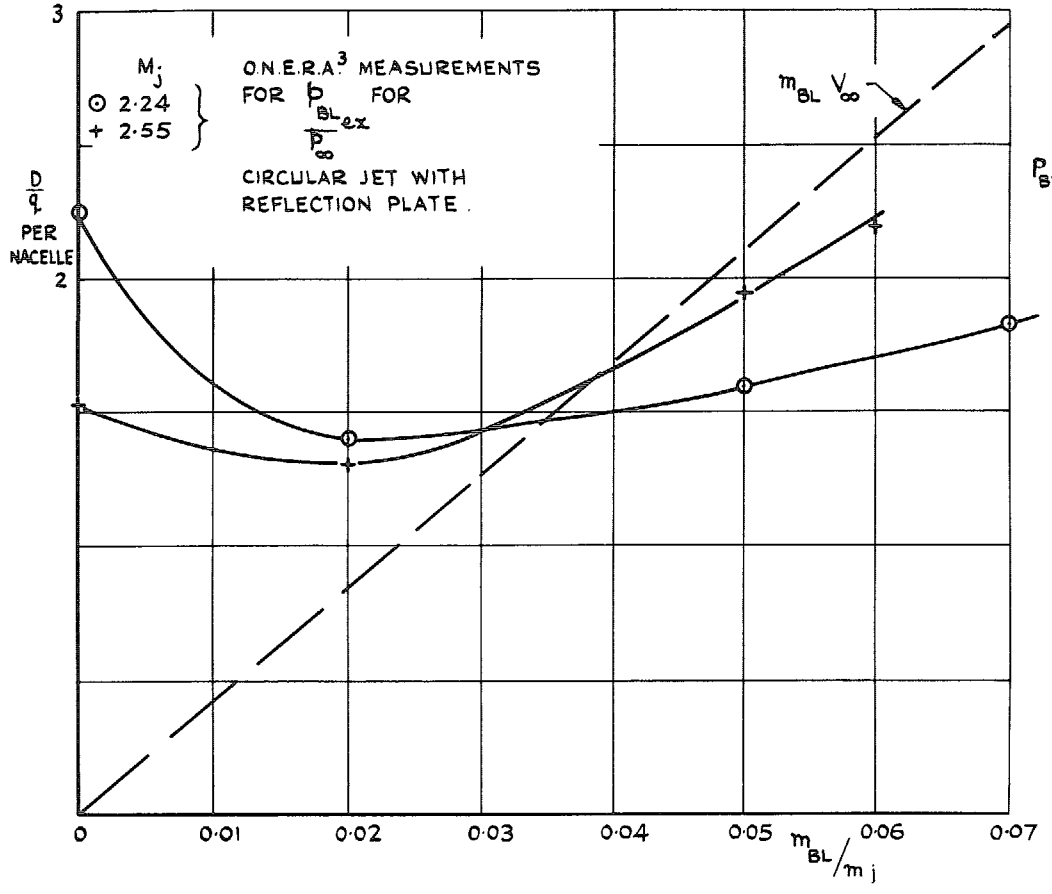

FIG. 16. Variation of bleed drag with bleed mass flow.

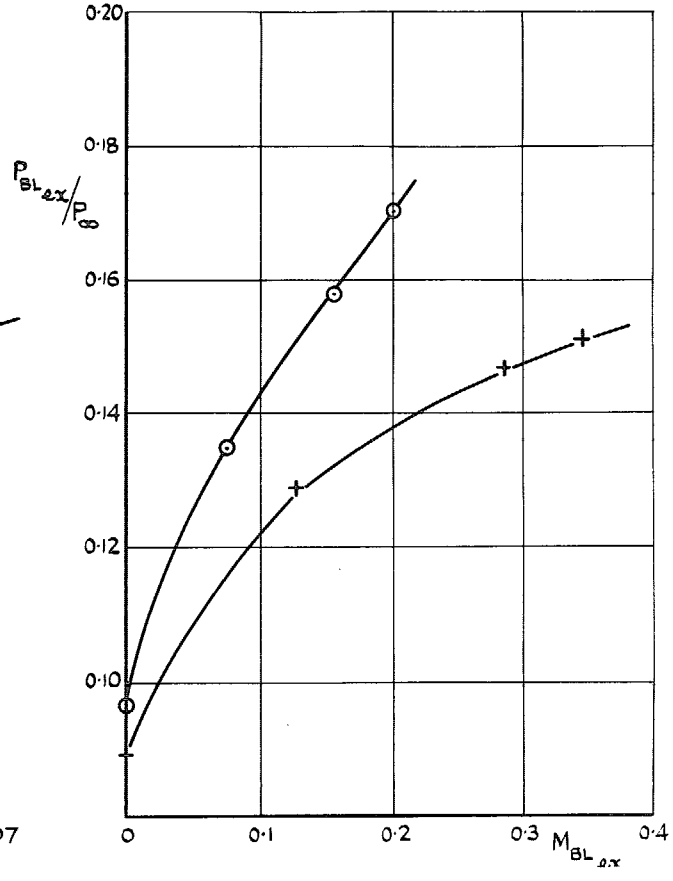

FIG. 17. Bleed-exit total pressure and Mach Number.

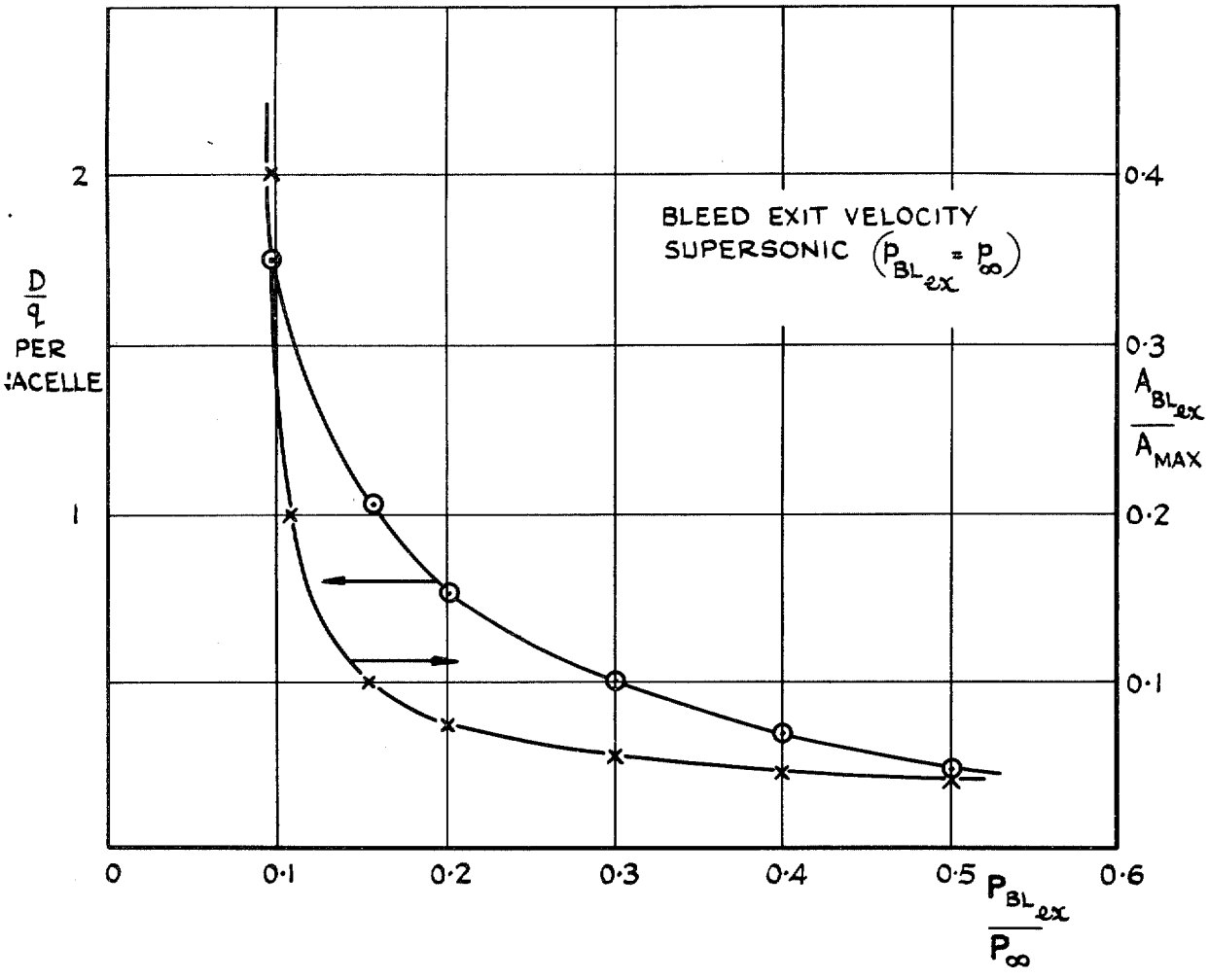

FIG. 18. Variation of drag and bleed exit area with bleed pressure recovery.

Printed in Wales for Her Majesty's Stationery Office by Allens Printers (Wales) Limited
Dd 129527 K5

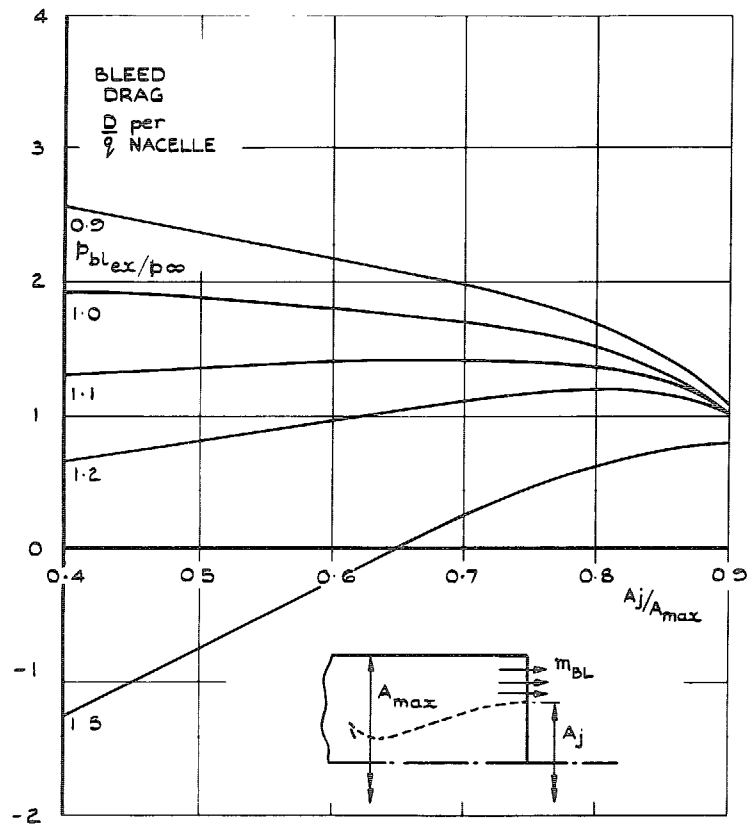

FIG. 19 (a)

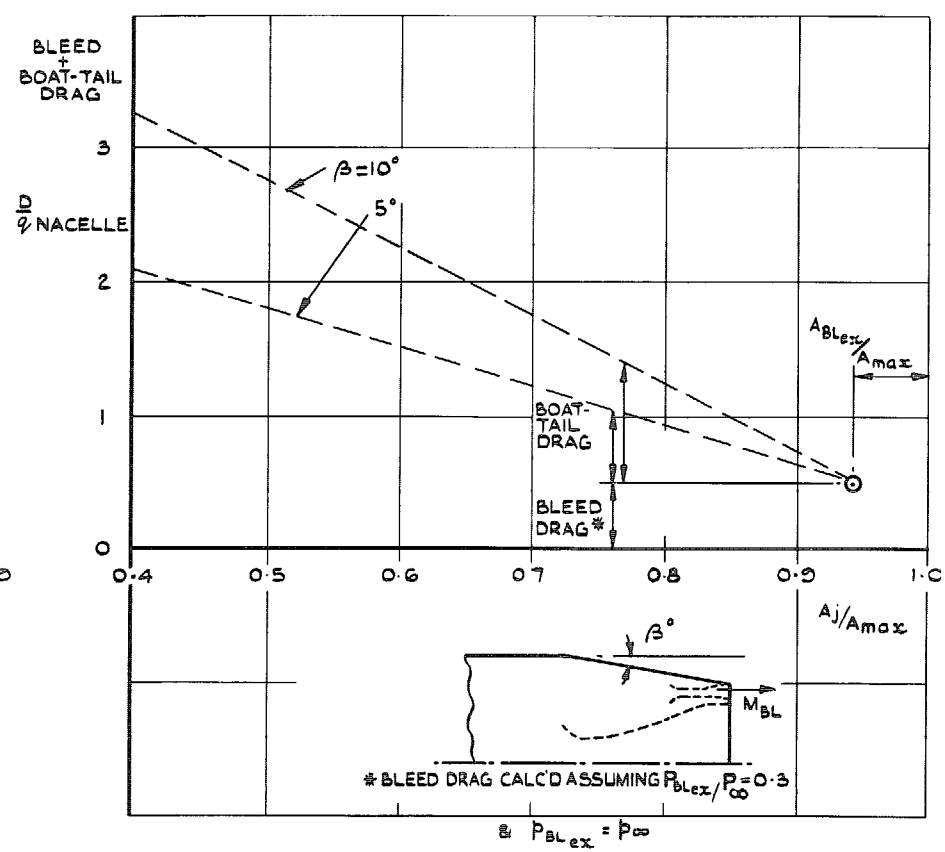

FIG. 19 (b)

FIG. 19. Comparison of drag for (a) low speed (no boat-tail) and (b) high speed (with boat-tail) ejection of bleed air.

Published by
HER MAJESTY'S STATIONERY OFFICE

To be purchased from
49 High Holborn, London W.C.1
423 Oxford Street, London W.1
13A Castle Street, Edinburgh 2
109 St. Mary Street, Cardiff
Brazennose Street, Manchester 2
50 Fairfax Street, Bristol 1
258-259 Broad Street, Birmingham 1
7-11 Linenhall Street, Belfast 2
or through any bookseller

S.O. Code No. 23-35